Microstructural influence on critical currents and irreversibility line in melt-textured $YBa_2Cu_3O_{7-x}$ reannealed at high oxygen pressure

J. Plain*
Institut de Ciència de Materials de Barcelona, CSIC, Campus U.A.B., 08193 Bellaterra, Spain
and Laboratoire de Métallurgie Physique, UMR 6630, Université de Poitiers, SP2MI, 86962 Chasseneuil Futuroscope Cedex, France

T. Puig, F. Sandiumenge, and X. Obradors
Institut de Ciència de Materials de Barcelona, CSIC, Campus U.A.B., 08193 Bellaterra, Spain

J. Rabier
Laboratoire de Métallurgie Physique, UMR 6630, Université de Poitiers, SP2MI, 86962 Chasseneuil Futuroscope Cedex, France
(Received 13 March 2001; published 4 March 2002)

We present a study of flux pinning by in-plane partial dislocations in melt-textured grown $YBa_2Cu_3O_7/Y_2BaCuO_5$ (123/211). The in-plane dislocations are generated by high oxygen pressure (HOP) postprocessing treatment as confirmed by transmission electron microscopy (TEM). In order to characterize the dislocation density and the perimeter to surface ratio (PSR) of the associated stacking faults a large number of TEM micrographs have been analyzed. We demonstrate that the evolution of the microstructure correlates with the oxygen absorbed by the samples during different HOP treatments. Two regimes of oxygenation activity are identified: first, the low oxygenation regime where the PSR of the stacking faults stays almost constant but the in-plane dislocation density is increased near the 123/211 interfaces and second, the high oxygenation regime where the stacking faults extend over the entire 123 matrix inducing a drastic enhancement of the dislocation density and a strong decrease in the PSR. Two contributions to the critical current density have been identified and quantified: the weak pinning and the correlated disorder pinning. We demonstrate that the correlated disorder comes from 123/211 interfaces and that this remains invariant with the HOP process. On the other hand, the weak pinning contribution is associated to the in-plane dislocations and this contribution strongly correlates with the HOP treatments. The temperature and field dependencies of the in-plane dislocations' contribution to the critical currents are in agreement with a pointlike single vortex pinning mechanism. Finally, we demonstrate that the dislocation pinning can be counterbalanced by wide stacking faults inducing a downward shift of the irreversibility line.

DOI: 10.1103/PhysRevB.65.104526 PACS number(s): 74.60.Ge, 74.60.Jg, 74.80.Bj

I. INTRODUCTION

It is well known that the microstructure characteristics of melt-textured grown (MTG) $YBa_2Cu_3O_{7-\delta}/Y_2BaCuO_5$ (123/211) composites dominate their physical properties. Thus, the understanding and control of the microstructure are interesting challenges for the improvement of the physical properties of MTG 123/211 and its applications. Since the beginning of the 1990s, many experiments have been performed in this view. The texturing of $YBa_2Cu_3O_{7-\delta}$ (YBCO) (123) allowed to reduce the limitation of the critical currents associated to high angle grain boundaries.[1] However, in spite of this advance, the gap existing between MTG 123/211 and optimized epitaxial thin films is still quite important. MTG 123/211 is a ceramic composite material with 211 particles embedded into the matrix and has a wide spectrum of defects (twin boundaries, subgrain boundaries, stacking faults, dislocations, and microcracks) which have a strong influence on the mechanical and superconducting properties. With the purpose of optimizing the superconducting properties of MTG 123/211, different approaches have been explored such as plastic deformation[2,3] and the addition of nonsuperconducting phases.[4,5] In particular, the effects of 211 inclusions have been intensively studied[6,7] but the subject is still much debated. Indeed, some authors have suggested that the pinning enhancement comes from the 123/211 interfaces[7] while others claim that pinning comes from the defects associated to the 123/211 interfaces.[8] Another controversy is the capability of the stacking fault as a pinning center. Some works have suggested that an increase of the stacking fault density induces an enhancement of pinning effectiveness.[9] But on the other hand, other authors have proposed that the in-plane dislocations associated to the stacking faults are the real pinning centers,[10,11] and that there is a competition effect between the stacking fault and its associated dislocations.[12,13]

We have previously shown[11] that high oxygen pressure (HOP) postprocessing treatments allow to increase the critical current density up to 180% for the optimized conditions. This strong enhancement is correlated with the generation of in-plane partial dislocations at the 123/211 interfaces.

In this work, we report a thorough analysis of the microstructural changes under HOP postprocessing treatments and their correlation with the pinning mechanisms. These changes are associated with the oxygenation activity under strong nonequilibrium conditions (i.e., with the oxygen available in the sample during the HOP postprocessing treatment required to transform the 123 phase into a local 124 and nucleate stacking faults). Transmission electron microscopy (TEM) observations do not reveal other important

changes of the microstructure. Thus, we have obtained by carrying out different HOP postprocessing treatments a set of samples with different in-plane dislocation density and perimeter to surface ratio (PSR) of stacking faults while keeping the 211 content constant. Assuming that the critical current density is the sum of different pinning contributions, we correlate these contributions with the observed defects. We clearly settle that interface pinning and in-plane dislocations associated to the interface have a distinguishable contribution to the critical currents and that the dislocation effect can be counterbalanced by wide stacking faults.

II. EXPERIMENT

MTG-YBCO samples with 30 wt.% of 211 were grown using a top seeding technique described elsewhere[14] followed by an oxygenation process at 1 bar and 450 °C for 120 h. Single domain pieces having typical dimensions $0.3\times0.3\times0.3$ cm^3 were cut from the bulk pellets and submitted to additional HOP treatments under constant pressure $P_{O_2}=100$ bar. In a first set of samples the HOP process was carried out at a temperature of 600 °C for a period of time ranging from 1 to 12 h. In a second set of samples, the time process was kept constant at $t=12$ h, while the process temperature was varied at $T=350$ °C, 450 °C, and 600 °C. These HOP samples are called H6001h, H6002h, H60012h, H35012h, and H45012h, respectively. The content of the 211 phase in the composite was confirmed by measuring the paramagnetic susceptibility of the sample and fitting a Curie-Weiss law in the high-temperature range ($T\geqslant120$ K).[7]

Inductive critical currents and irreversibility lines were deduced from magnetization measurements performed with a superconducting quantum interference device magnetometer using a 3 cm scan length to avoid field inhomogeneity. The typical size of the samples used in these magnetization measurements was $1.5\times0.8\times0.5$ mm^3. The longest dimension (c axis) was placed parallel to the magnetic field in order to minimize demagnetizing effects. The critical current was calculated from the generalized Bean critical state model,

$$J_c^{ab}=\frac{20\times\triangle M}{l_1\times\left(1-\frac{l_1}{3\times l_2}\right)\times V}, \tag{1}$$

where $l_1\leqslant l_2$ are the sides limiting the surface perpendicular to the applied field, $\triangle M$ is the difference between the upper and the lower branches of the $M(H)$ hysteresis loops, and V is the sample volume.[15,16] The irreversibility line was deduced from zero-field cooled (ZFC)-field cooled (FC) magnetization measurements as a function of temperature. The irreversibility field was obtained from the criterion

$$\frac{M_{ZFC}-M_{FC}}{M_{ZFC}}=0.01, \tag{2}$$

which corresponds to a critical current equivalent criterion of $\sim10-100$ A/cm^2. The microstructure of the samples was characterized using Philips CM30 and Jeol 200CX electron microscopes operated at 300 keV and 200 keV, respectively. TEM samples were cut parallel and perpendicular to (001). They were mechanically polished down to 30 μm and further ion milled down to 100 nm at reduced voltages (4.5 kV) and currents (0.3 mA) using a cold finger immersed in liquid nitrogen to avoid damage of the microstructure.

III. RESULTS AND DISCUSSIONS

A. Microstructural changes under a HOP process

Under HOP conditions the 123 phase is highly unstable and decomposes into a mixture of 211, Ba-Cu oxide, and CuO according to the reaction[17,18]

$$4YBa_2Cu_3O_{7-x}+\left(\frac{1-3\delta}{2}+2x\right)O_2 \rightarrow 2Y_2BaCuO_5+3Ba_2Cu_3O_{6-\delta}+CuO. \tag{3}$$

At the same time the 124 phase is more stable than the 123 +CuO mixture. Accordingly, during a HOP process, the CuO released during the decomposition of the 123 phase [Eq. (3)] can be inserted in the 123 matrix as intrinsic stacking faults. Thus, locally the 124 phase may be generated by the insertion of a double CuO_x chain layer.[19] The massive formation of stacking faults is the principal microstructural change during the HOP process. The extent of this transformation and in particular the shape and size of these stacking faults are found strongly dependent on the temperature and time of the postprocessing treatment. In order to compare the different HOP treatments, we define the magnitude of oxygenation activity, ΣO_2, as the oxygen available in the sample for the phase transformation described by Eq. (3). This quantity is given by

$$\Sigma O_2=C_0\int_0^t dt\int_0^z dz\ \mathrm{erfc}\frac{z}{2\sqrt{Dt}}, \tag{4}$$

where C_0 is a normalizing constant depending on the applied oxygen pressure, t the process time duration, z the depth of the sample, and D is the diffusion coefficient. D is given by

$$D=D_0e^{-U/kT}, \tag{5}$$

where U is the activation energy, k the Boltzmann constant, and T the temperature of the HOP process. We have calculated the diffusion parameter D considering that the diffusion along the c axis is negligible (i.e., $D_{ab}\gg D_c$). Note that the erfc(x) function in Eq. (4) is the solution for the diffusion equation[20,21] indicating the oxygen concentration profile in the samples. Hence, ΣO_2 provides a dimensionless parameter characterizing the total oxygen uptaken by the sample during the various HOP treatments.

1. High oxygen pressure processed at 350 °C *and* 450 °C

TEM observations did not reveal significant microstructural differences between samples processed at 350 °C and 450 °C. Observations around the [001] viewing direction revealed a high increase in the dislocation density preferentially around the peritectic 211 particles, while the regions between the particles remained almost defect-free. Figure 1 shows a bright field electron micrograph of the (001) plane

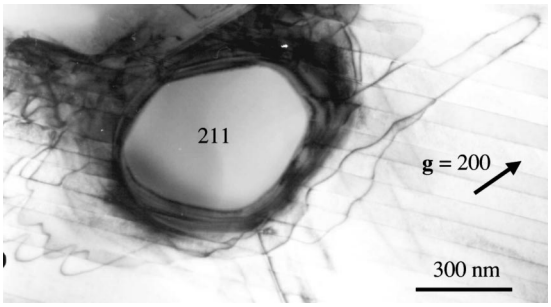

FIG. 1. Bright field electron micrograph ($g=200$) of the (001) plane of the sample postprocessed at 450°C showing a high partial dislocation density around one 211 inclusion. Note that the dislocations are principally aligned along the [100] direction.

taken with the diffraction vector $g=200$ of a matrix region around two 211 particles. A significantly high density of dislocations around the particles which suddenly drops with the distance from the interfaces is clearly observed. The same area is shown in Fig. 2 under $g=110$. Note that in this case, the regions enclosed within the dislocations display stacking fault contrast (dark contrast). The observed contrast is in fact that expected for stacking faults with a $1/6\langle 301\rangle$ displacement vector, typically found in 123 materials,[22–24] which consist of the intercalation of an extra CuO_x chain layer between the two adjacent BaO atomic layers.[25] Note that such stacking faults are thus equivalent to a local 124-type structure. By inspection of the micrographs it can be concluded that within the thickness of the sample TEM foil (~ 100 nm), several stacking faults are superposed along the viewing direction, i.e., the *c* axis of the matrix. The shape of the stacking faults is highly anisotropic, thus indicating the occurrence of a preferential growth direction along the [100] and [010] directions, i.e., at 45° from the twins (since the contrast features do not change across the twin boundaries, the notation $\langle 100\rangle$ will be used for [100] and [010]).

From the above results, it can be concluded that upon HOP treatments at these temperatures (i.e., 350 °C and 450 °C), only the microstructure around the 211 particles is modified by the nucleation and rapid growth of 124-type extrinsic stacking faults, in a similar way as previously observed in samples aged for several days under flowing oxygen.[26] The main difference is that in this case the size of the faulted areas is much smaller while the density of stacking faults along the *c* axis is kept very high. A rough estimation of the growth rate of the stacking faults from TEM micrographs indicates that it is about one order of magnitude higher at 100 bar (~ 100 nm/h) than at 1 bar of oxygen. This rapid growth, along with the highly anisotropic growth shape, leads to stacking faults having an enhanced perimeter (length of the bounding partial dislocation) to surface ratio. Partial dislocation density within a distance of 400 nm from the 211 particles may reach values up to 2×10^{10} cm^{-2}.

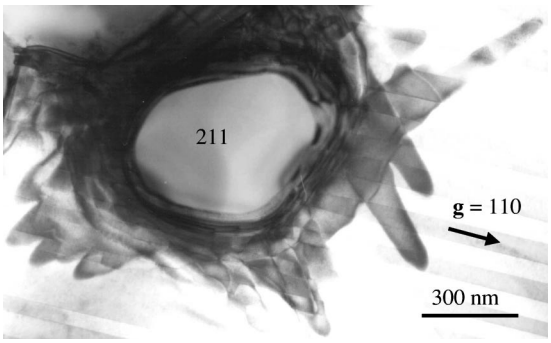

FIG. 2. Same area as in Fig. 1 taken with $g=110$. Stacking faults elongated in the $\langle 100\rangle$ directions appear dark.

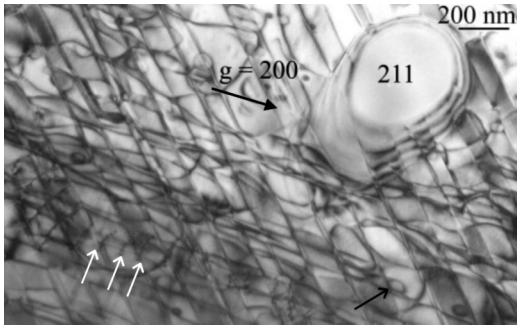

FIG. 3. Microstructure after HOP at 600 °C during 12 h. Bright field electron micrograph ($g=200$) of the dislocation substructure on the (001) plane. Note that the dislocation density around the 211 particle is lower than in the bulk matrix. Arrowheads show a set of dislocations lying out of the glide plane. Faulted dislocation loops are indicated by the black arrow.

2. High oxygen pressure processed at **600°C**

When the HOP treatment is performed at 600 °C, the microstructure undergoes dramatic changes relative to that described for the low-temperature processed samples. Observations of the (001) plane reveal an important increase in the dislocation density, up to 2.5×10^{10} cm^{-2} within the bulk matrix that is not preferentially associated to the 211 particles. This feature is clearly observed in the $g=200$ electron micrograph of the (001) plane, presented in Fig. 3.

Note that the dislocation density is even higher within the bulk matrix than around the 211 particle. The wide dark fringes around the 211 particle are depth fringes, which are commonly observed at incoherent boundaries when the two overlapping phases scatter the incident beam with different intensities. Similar to the samples processed at 350 °C and 450 °C, the dislocations are aligned with the $\langle 100\rangle$ directions. A further distinctive feature clearly shown in Fig. 3 is the occurrence of circular or elliptic partial dislocation loops isolated within the matrix, as indicated by arrows in the image. Striking images taken with $g=110$, in order to image the faulted areas, displayed dark stacking fault like contrast throughout all the bulk matrix, thus signaling that within the thickness of the TEM specimen, wide areas larger than ~ 10 μm^2 are covered by overlapping stacking faults along the *c* axis. The same image (i.e., Fig. 3) also shows a set of dislocations lying out of the (001) plane, as indicated by arrowheads. The oscillatory contrast displayed by these dislocations is that expected for dislocation lines inclined to the foil surface,[27] which in this sample is close to the (001) plane. Such out-of-plane dislocation arrangements are ex-

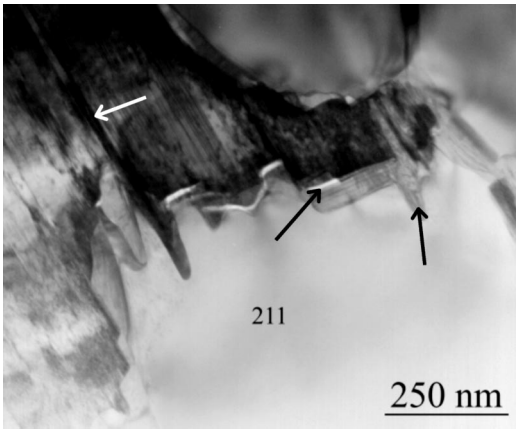

FIG. 4. Reactive interface, viewed along the [100] zone axis of the matrix. Note that the 211 particle displays short arms extending in the direction of the (001) matrix planes. Secondary inclusions at the 123/211 interface are indicated by black arrows. A microcrack is indicated by the white arrow.

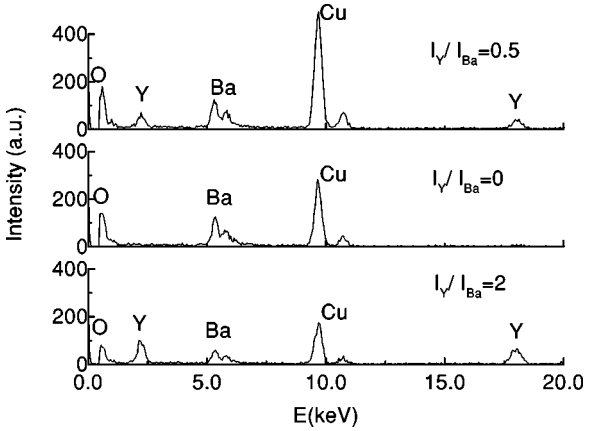

FIG. 5. Comparison of EDX analyses taken in the (a) 123 matrix, (b) secondary phase, and (c) 211 inclusion. Notice that the secondary phase is yttrium-free.

pected to build up by a climbing process in samples processed at high temperatures, when diffusion-assisted dislocation movements are most likely to occur.[28] In order to observe the microstructure along the *c* axis, TEM observations were also performed on planes perpendicular to (001). An example is presented in Fig. 4 showing an electron micrograph taken along the [100] (or [010]) viewing direction, i.e., the (001) planes are perpendicular to the image. The micrograph shows a matrix area between two neighboring 211 particles displaying an irregular interface. By analysis of several images it was concluded that the tiny straight lines correspond to stacking faults viewed edge on, stacked along the *c* axis. The huge density of stacking faults observed in this projection is indeed consistent with the generalized stacking fault contrast observed throughout the matrix in the observations of the (001) plane (Fig. 3). Now, turning to the features displayed by the 211 particle, one can observe that it presents an irregular shape with short arms extending parallel to the (001) planes of the 123 matrix, strongly suggesting a reactive interface. Indeed, between the 211 particle and the matrix, a secondary phase indicated by black arrows, displaying a distinctive contrast, is also observed (white ribbons correspond to holes left by small particles presumably eliminated during the ion milling process). Electron dispersive x-ray (EDX) analyses indicated that the secondary phase is a Ba-Cu oxide, though we did not succeed in the determination of its precise stoichiometry. Figure 5 compares the EDX analyses obtained from the 211, 123, and secondary phases. The height of the Cu peak is affected by electrons dispersed by the Cu grid supporting the sample and therefore cannot be used to estimate the cation composition. However, the results clearly reveal that the secondary phase is Y-free, and contains Ba and Cu in good agreement with Eq. (3).

3. Microstructure development under HOP

Under HOP, the microstructure development is governed by the interplay of plastic deformation and phase instability. Under an isostatic pressure, plastic deformation results from the anisotropy of the elastic constant of the 123 matrix[29] and the plastic anisotropy between the 211 particles embedded on the 123 matrix.[30] However in this case, the most relevant driving force for the generation of the observed microstructures comes from the instability of the 123 phase and the tendency towards the nucleation of the 124-like stacking faults. It was clearly shown that under HOP,[19] the 123 phase is brought far from its stability field and at the same time the 124 phase is stable against a 123+CuO mixture. Early studies on ceramic powders showed that on the HOP region of the phase diagram, the 123 phase decomposes to a mixture of 211, a Ba-Cu oxide, and to a lower extent CuO and occasionally 124.[17,18] Since the same region of the phase diagram corresponds to the stability field of 124, the nucleation of 124-like stacking faults can be interpreted as a local phase transformation of 123 to 124,[31] in which the CuO is supplied by the local decomposition of 123. As pointed out in such studies,[17,18] the decomposition does not take place homogeneously but is preferentially activated at the grain boundaries, i.e., high stress regions in the ceramic powder.

Indeed, the microstructures observed by TEM in our melt-textured samples are easy to reconcile with the above scenario. In the high-temperature-long-time regime (600 °C, 12 h), where the microstructure has developed to a larger extent and can therefore be used to magnify the mechanisms operating under softer conditions, we found that the decomposition of the matrix takes place preferentially at the 211 interfaces. There are several factors that make these places the most favored ones for the decomposition: first, owing to the plastic and thermal mismatch between the 123 matrix and 211, their interface is very likely to provide stress conditions for the activation of the decomposition. Second, 211 also constitutes one decomposition product and can therefore nucleate and grow on the preexisting particles.

A further feature of the microstructure generated in the high-temperature regime is a dramatic increase in the size of the stacking faults, such that within the thickness of the TEM thin foil ($\sim$100 nm), areas $\geqslant 10\ \mu m^2$ appear completely covered by faults overlapped along the *c* axis. At the same time, the dislocation density is enhanced within the bulk matrix, and in contrast to the samples processed in the low-

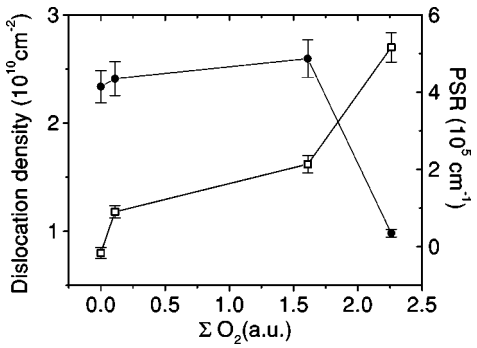

FIG. 6. (□) Dislocation density and (●) perimeter to surface ratio of the stacking faults quantified from TEM micrographs as a function of the oxygenation activity.

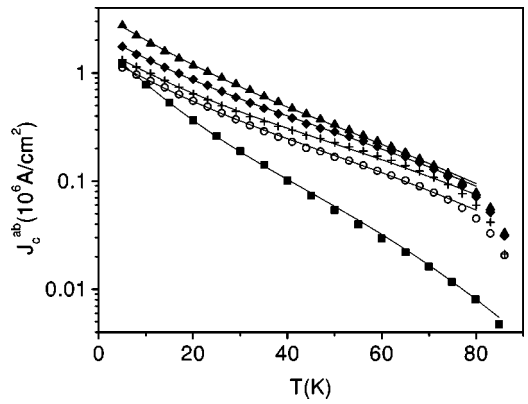

FIG. 7. Temperature dependence of the self-field critical current density for H parallel to the [001] direction, J_c^{ab}, for (○) virgin, (+) H60012h, (♦) H6002h, (▲) H35012h, and (■) single crystals. Note the different behavior between the single crystal and the MTG 123/211 samples. Lines are fits of $J_c^{ab}(T)$ describing the sum of both contributions, i.e., weak pinning and correlated disorder pinning [see Eq. (8)].

temperature regime, it becomes no longer associated to the 123/211 interfaces. These features can be understood taking into account that most of the dislocations introduced by HOP are partials bounding the stacking faults that move away from the interfaces as they grow on the (001) plane. In fact, observations of the microstructure on planes perpendicular to (001) indicate an extremely high density of faults stacked along the *c* axis, such that the growth of additional stacking would be presumably impeded by interactions with the stress field associated to the neighboring ones. In this scenario, additional mechanisms for the nucleation of the 124-like stacking faults are required, such as the nucleation on certain sites within the bulk matrix providing the necessary stress and feeding conditions. This would explain the unusual occurrence of faulted loops distributed in the bulk matrix. The microstructure observed after the low-temperature treatments (350 °C and 450 °C) and the high-temperature treatment during a short time can be considered as an incipient stage in the process of microstructural development under HOP. Unlike in the sample processed at 600 °C during 12 h, here the microstructure appears dominated by the nucleation of a high density of small stacking faults at the 123/211 interfaces and within the matrix when the interfaces are locally saturated. In this case, our observations indicate that the 211 particles act as multinucleation sites for 124-like stacking faults. In this way, the dislocation density around the particles may peak up to 2×10^{10} cm^{-2} while it suddenly drops down to zero within the bulk matrix. The high growth shape anisotropy combined with the strong nonequilibrium growth conditions under HOP, result in a two-dimensional analogue of a dendritic shape of the stacking faults (Fig. 2) that maximizes the total length of partial dislocations bounding the stacking faults.

In order to summarize the microstructural changes for the different regimes, TEM image analyses have been performed. Thus, we have calculated the dislocation density and the PSR of stacking faults for the virgin sample and samples in the two different ΣO_2 regimes (i.e., H6001h, H45012h for the low oxygenation regime and H60012h for the high ΣO_2 regime). The results are shown in Fig. 6. First, we see that the dislocation density increases with the oxygenation activity. Second, the PSR stays almost constant for the low oxygenation regime but decreases strongly for the high value of ΣO_2. These results are coherent with the scenario presented above. Indeed, in the low oxygenation regime, there is creation of highly dendritic stacking faults situated generally at the 123/211 interfaces and in the high oxygenation regime, there is an expansion of large stacking faults extending to the entire matrix.

B. Critical current densities and irreversibility lines

1. Defect contributions to the temperature dependence of J_c

Figure 7 shows the temperature dependence of the critical current density J_c^{ab} for the $H//c$ axis measured in self-field conditions, for samples postprocessed at different temperatures and times. A single crystal is also shown for comparison. First of all, a comparison between samples shows that the critical current density of the postprocessed samples has increased for all the temperature range (up to 180% for sample H35012h at 5 K) if compared to the virgin sample. Furthermore, notice that all the samples present the same behavior in the temperature dependence of J_c for temperatures above 35 K except the single crystal. Indeed, melt-textured 123/211 composites have been shown to exhibit a change in the dominating pinning mechanism due to the presence of 123/211 interfaces[7] or associated defects[8] above ~35 K.

In order to study and separate the influence of the defects on the critical current density, we consider two relevant contributions to flux pinning: weak pinning centers (WPC's), which will mainly be associated to in-plane dislocations, and correlated disorder (CD) which will account for the 123/211 interfaces. The temperature dependence of the critical current density for weak pinning centers is that typically observed in 123 single crystals[32] and may be described by[33]

$$J_c(T)=J_{WP}\times e^{-T/T_0}. \tag{6}$$

Instead, correlated disorder theory was first developed for the contribution coming from columnar defects generated by

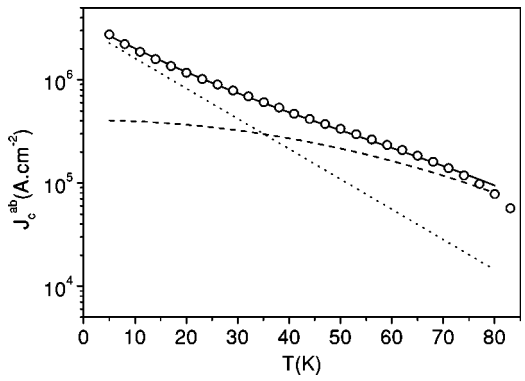

FIG. 8. Thermal dependence of the measured critical current density for the (○) H35012h sample and contributions coming from (dots) weak pinning centers, (dashes) correlated disorder, and (line) the sum of both given by Eqs. (6)–(8), respectively.

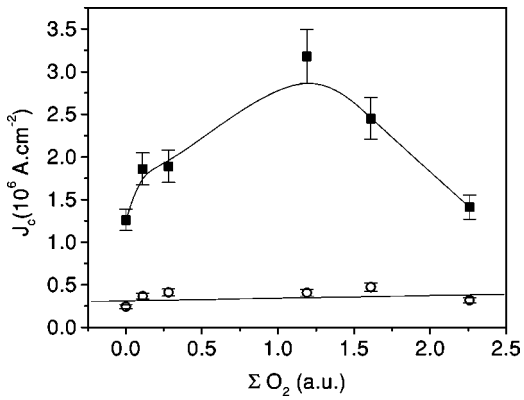

FIG. 9. Calculated critical current density at 0 K for (■) weak pinning center J_{WP} and (○) correlated disorder J_{CD} as a function of ΣO_2. Solid lines are guides for the eyes.

heavy-ion irradiation and twins in 123 single crystals,[34] but it was shown that this theory could also well describe the critical current behavior of 123/211 interfaces in MTG composites:[7]

$$J_c(T) = J_{CD} \times e^{-3(T/T^*)^2}. \tag{7}$$

The measured self-field temperature dependence of the critical current density of MTG should account for the sum of the above two contributions:

$$J_c(T) = J_{WP} \times e^{-T/T_0} + J_{CD} \times e^{-3(T/T^*)^2}, \tag{8}$$

where J_{WP} and J_{CD} are the critical current densities at 0 K for weak and correlated disorder, respectively, and T_0 and T^* are characteristic temperatures which fix the energy scale of the pinning centers for each contribution. Figure 7 shows the raw data of the samples perfectly fitted by Eq. (8) up to 80 K where a sharp drop occurs due to the proximity of the irreversibility line. From these global fit results, we have calculated the separate contribution coming from Eqs. (6) and (7) for weak and correlated disorder contributions, respectively. Figure 8 presents the raw data, the global fit, and the two separated contributions for the H35012h sample. Notice that weak pinning is dominant at low temperatures, while above 35 K there is an inversion of the weights from the WPC contribution to the CD contribution. Thus, above 35 K the dominant contribution comes from the correlated disorder generating the characteristic bump observed by Martinez *et al.*[7] in the temperature dependence of the critical current density of MTG-YBCO samples. As shown in the microstructural observations, we have modified the dislocation density at a constant 211 concentration. Thus, we can perform an analysis of the influence of the in-plane dislocations on the critical current density. We have used the above methodology to separate the contributions coming from the WPC and CD. We correlate the microstructural changes via the oxygenation activity parameter. Figure 9 shows the ΣO_2 dependence of the critical current densities at 0 K for both contributions J_{WP} and J_{CD}. It can be noted that J_{WP} is strongly modified by oxygenation while the correlated disorder parameter, J_{CD}, remains almost constant. An increase of about 180% in J_{WP} is achieved at $\Sigma O_2 \simeq 1.2$ as compared to the virgin sample where J_{WP} reaches 3×10^6 A/cm^2. For higher ΣO_2 values, J_{WP} decreases and reaches a value similar to that of the virgin sample for $\Sigma O_2 \simeq 2.2$. In MTG 123/211 the defects that may contribute to correlated disorder are twin boundary and 123/211 interfaces. It has been proven that twin boundary pinning contributes to J_c for $H//[110]$,[6,35–37] and to the vortex liquid viscosity[38] for $H//c$. Unfortunately, there is no quantification of the twin boundary pinning contribution in the solid vortex state when $H//c$ in spite of Suematsu *et al.*, who have shown experimentally that twin boundaries act as pinning centers.[39] As TEM observations do not reveal changes in the twin boundary density, we will consider that their contribution stays constant in all our samples.

On the other hand, Martinez *et al.* have shown that 123/211 interfaces act as pinning centers and can be described by the correlated disorder theory,[34] though this subject is still strongly debated. Indeed, some authors claim that the defects associated to the 123/211 interface are responsible for pinning.[8] Our present results demonstrate that in the low ΣO_2 regime, the 211 inclusions and 123/211 interfaces were not modified during the HOP process as evidenced by TEM observations. However, a strong increase in the density of the defects associated to the 123/211 interface (i.e., stacking fault and associated dislocations) has been clearly found. From our results, it seems clear then that the defects created by the HOP treatment are weak pinning centers. Consequently, they do not play a role in the change of the temperature-dependence behavior of the critical current density occurring around 35 K generally associated to 211 inclusions.

On the contrary, in the high ΣO_2 regime a downward shift in the dependence of the critical current density is observed in spite of a drastic increase in the dislocation density in the entire 123 matrix, indicating that the in-plane dislocation contribution can be counterbalanced by a high density of wide stacking faults.

2. Defect contributions to the field dependence of J_c and the irreversibility line

We have studied the influence of in-plane dislocations on the field dependence of the critical current density and the

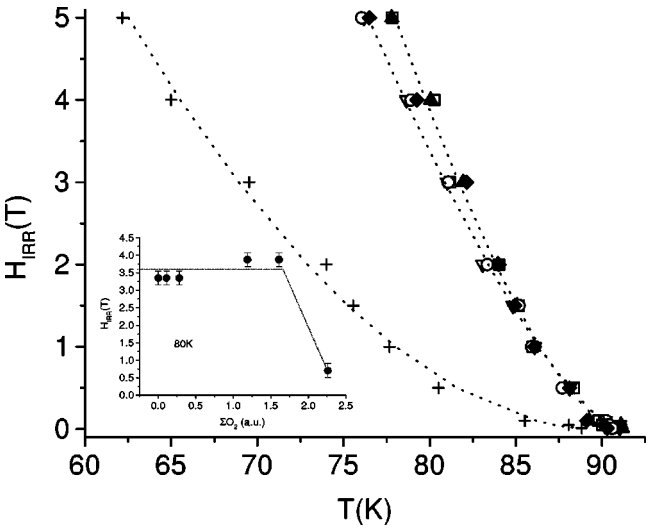

FIG. 10. Inductive irreversibility lines of (○) virgin, (+) H60012h, (▽) H6001h, (♦) H6002h, (□) H45012h, and (▲) H35012h samples. Dotted lines are fits coming from Eq. (9). The inset shows the irreversible field versus the oxygenation activity for a temperature of 80 K.

irreversibility line when the field is applied parallel to the c axis. The irreversibility lines for all the samples are displayed in Fig. 10. The dotted lines are fits of the irreversibility line given by

$$H_{\mathrm{IRR}} \equiv H_0 \left(1 - \frac{T_{IRR}}{T_c} \right)^{\alpha}, \tag{9}$$

where H_0 and α are the fitting parameters corresponding to the irreversibility field at 0 K and to temperature dependence of the irreversibility field, respectively. Notice that there is no relevant difference between the irreversibility lines of the low ΣO_2 regime samples and the virgin one. On the other hand, in the case of the high ΣO_2 regime sample, the irreversibility line is shifted to lower temperatures. In the inset, we plot the irreversibility field at 80 K as a function of ΣO_2. The difference between the low ΣO_2 regime samples and the virgin is quite low ($\Delta H_{\mathrm{IRR}} \leqslant 0.5$ T at 80 K). We conclude that the newly generated in-plane dislocations and associated stacking faults do not modify the irreversibility line when the PSR of the stacking faults is not changed (i.e., a low ΣO_2 regime). On the other hand, H_{IRR} is strongly decreased for the high ΣO_2 regime sample (i.e., $\Delta H_{\mathrm{IRR}} = 3$ T at 80 K). As shown by Sandiumenge *et al.*,[26] a strong decrease in the irreversibility line can be linked to the creation of wide stacking faults during a very long oxygenation process even at $P_{O_2} = 1$ bar. For the low ΣO_2 regime, the independence of the irreversibility line with the HOP process indicates that in-plane dislocations act as pointlike pinning centers when the field is applied parallel to the c axis.[40] In the case of the high ΣO_2 regime, the strong depression of the irreversibility line can be associated to the high density of wide stacking faults (the mean surface of the stacking fault $\geqslant 10$ μm^2) generated by the 123 phase transformation during the process. Therefore, the vortex correlation along the c axis is reduced because the 124 phase (i.e. the stacking fault) has an enhanced anisotropy and a lower T_c (Refs. 41 and 42) inducing a downward shift of the irreversibility line and, thus, depressing the efficiency of in-plane dislocations as pinning centers.

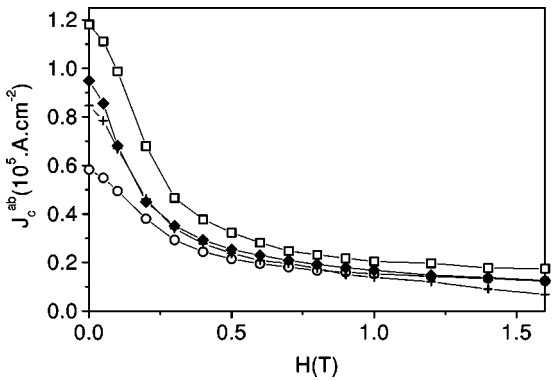

FIG. 11. Magnetic-field dependence of the inductive critical current density measured at 77 K for (○) virgin, (+) H60012h, (♦) H6002h, and (□) H45012h samples. Note that the highest difference between samples is localized at low fields.

The field dependence of the critical current density at 77 K is plotted in Fig. 11. First of all, we want to remark that the critical current density is increased upon all the HOP treatments. At low fields ($B \leqslant 1.5$ T), we find the more relevant changes in J_c induced by the different treatments. Indeed, at high fields all the samples tend to the same limit (i.e., they all have the same irreversibility point as shown above) except for the critical current density of the high ΣO_2 regime sample which decreases quickly in agreement with the strong depression of the irreversibility line. At low fields, we can consider that the vortex-vortex interaction is negligible and that vortices are pinned individually on each defect. Thus, we assume a single vortex regime and a summation of the individual microscopic pinning forces may be performed leading to[6,43]

$$J_c^{ab} = \frac{\pi \xi_{ab} B_c^2 V/d}{4\mu_0 \phi_0^{1/2}} \times B^{-1/2} + \eta \frac{\pi B_c^2 N_d |b|^2}{4\mu_0 \phi_0^{1/2}} \times B^{-1/2} = \beta \times B^{-\alpha}, \tag{10}$$

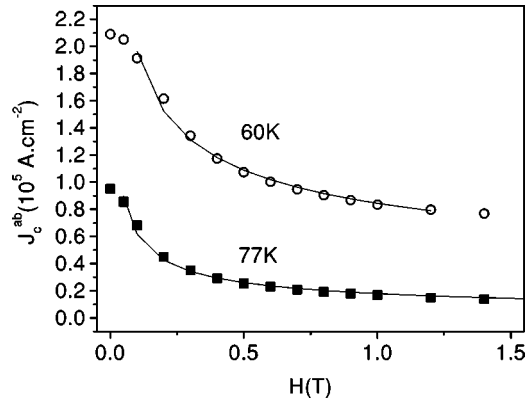

FIG. 12. Magnetic field dependence of the inductive critical current density for the H35012h sample at (○) 60 K and (■) 77 K. Lines are fits obtained from Eq. (10) describing pinning by 123/211 interfaces and in-plane dislocations within the single vortex regime.

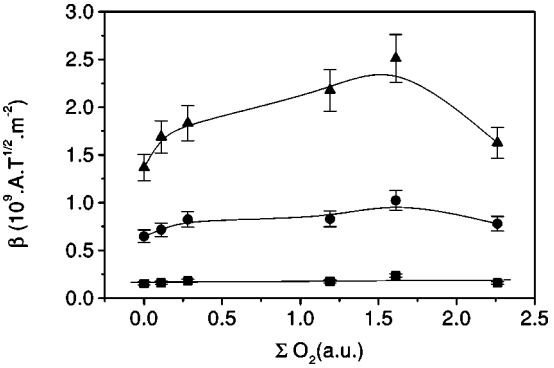

FIG. 13. Oxygenation activity dependence of the parameter β which is proportional to the number of pinning centers (i.e. 123/211 interfaces and in-plane dislocations) in Eq. (10) at (▲) 45 K, (●) 60 K, and (■) 77 K. Solid lines are guides for the eyes.

where ξ_{ab}, B_c, V/d, N_d, η, and b denote the coherence length in the ab plane, the thermodynamic critical induction, the 123/211 interface density, the dislocation density, a temperature-dependent weight parameter, and the Burgers vector, respectively. β is proportional to the number of pinning centers and α gives the field dependence of the critical current density, describing the pinning mechanism. We have fitted the raw data obtained for the critical current density with Eq. (10) for fields $\leqslant 1.5$ T as shown in Fig. 12 for two different temperatures. The dependencies of β and α with ΣO_2 are plotted in Figs. 13 and 14, respectively. We note that β decreases with temperature for all the samples. Indeed at 77 K, β is almost independent of ΣO_2 due to the quasinegligible contribution of in-plane dislocation compared to the 123/211 interfaces' contribution. On the other hand, at lower temperatures (i.e., 45 K and 60 K), the relevance of the in-plane dislocations as pinning centers induces a strong correlation between β and ΣO_2 (i.e., between the number of pinning centers and the oxygen available for the stacking fault

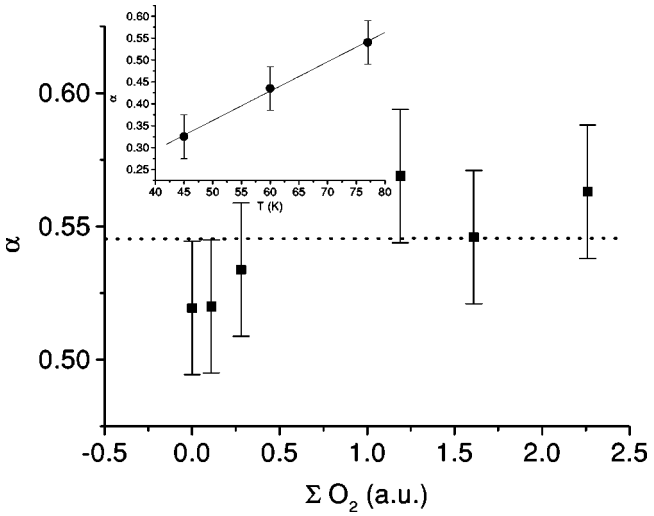

FIG. 14. Oxygenation activity dependence of the parameter α at 77 K associated to the pinning mechanism obtained from Eq. (10). In the single vortex regime, α is expected to be 0.5. Shown in the inset is the obtained temperature dependence of α.

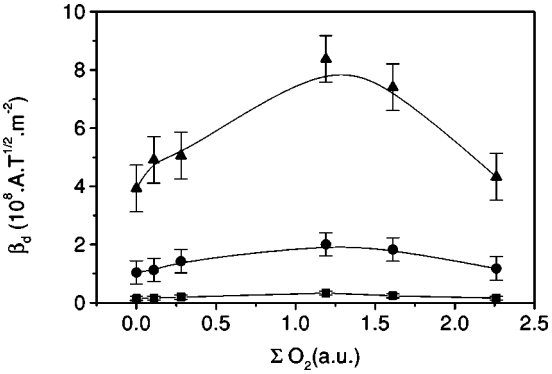

FIG. 15. Oxygenation activity dependence of the in-plane dislocation contribution to the parameter β estimated from the weak pinning contribution of the critical current-density temperature dependence at (▲) 45 K, (●) 60 K, and (■) 77 K. Solid lines are guides for the eyes.

creation). In order to separate both contributions (i.e., 123/211 interfaces and in-plane dislocations) in β, we have taken the weight of each contribution determined from the analysis of the temperature dependence of J_c shown in the previous section. The results obtained for the in-plane dislocation contribution β_d at 45 K, 60 K, and 77 K are plotted in Fig. 15 as a function of ΣO_2. Note that the in-plane dislocation contribution as a pinning center, as deduced from the field dependence represented by Eq. (10) (see Fig. 15) mimics that deduced from the analysis of the temperature dependence deduced from Eqs. (6) and (8) (see Fig. 9). Knowing the increase of dislocation concentration associated to the high $P\ O_2$ annealing, we can quantitatively evaluate the second term in Eq. (10) and particularly estimate the η parameter which measures the efficiency and extent of core pinning and the flux-line lattice rigidity. The estimated η values range from 1.5 at 77 K to 4.5 at 45 K. We have then calculated β_d for the H45012h sample and the virgin one from the theoretical Eq. (10) for each temperature. These values have been compared to the experimental estimations. As can be ob-

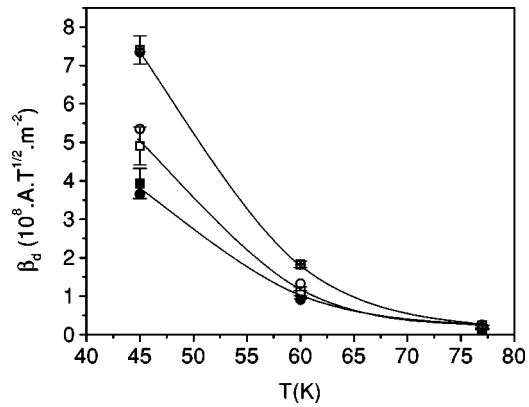

FIG. 16. Temperature dependence of the β_d which represents the in-plane dislocation contribution calculated theoretically (circles) and deduced from experimental measurements (squares) for H45012h (+ center symbols), H6001h (open symbols), and the virgin sample (solid symbols). Note the good agreement between theory and experimental results. Black lines are guides for the eyes.

served in Fig. 16, the experimental results are in excellent agreement with the theory. This further confirms the validity of our flux pinning model in separating 211 and in-plane dislocations contributions. In all cases, the exponent α was found to be independent of ΣO_2 (see, for instance, Fig. 14 at 77 K) and approximately 0.55 for all the samples, which is in good agreement with the expected 0.5 of Eq. (10). In the inset, the mean value of α is plotted as a function of temperature. We remark that though α decreases with the temperature, it is in good agreement with the theory at high temperatures (i.e., $T=77$ K, $\alpha \simeq 0.5$). Therefore, the assumption of a single vortex regime at low fields is verified for high temperatures. The origin of the temperature decrease of α is still unclear but might be related to an increase of the flux-line lattice rigidity at lower temperatures.

IV. CONCLUSIONS

We have investigated the microstructural changes induced by HOP postprocessing treatments, which have been correlated with the temperature and magnetic-field dependence of the critical current density and irreversibility line. We have shown that under high oxygen pressure conditions, the microstructure can be strongly modified, principally the shape and the density of in-plane partial dislocations. In order to quantify the oxygen quantity penetrating into the sample during the HOP process, we have defined the magnitude of oxygenation activity ΣO_2 as the oxygen available in the sample for the stacking fault creation. Two distinctive regimes of oxygenation activity were found: First, the low oxygenation regime, characterized by an increase in the in-plane dislocation density near the 123/211 interfaces with a constant perimeter to surface ratio of the stacking fault, and second, the high oxygenation regime, presenting a strong increase of the in-plane dislocation density in the entire matrix and a PSR of the stacking fault strongly depressed by the creation of wide stacking faults. From critical current-density and irreversibility line measurements, we have separated two pinning contributions: the weak pinning and the correlated disorder pinning. It is clearly settled that the new defects (i.e., stacking faults and in-plane dislocations) act as weak pinning centers and that the 123/211 interface contribution is described by the correlated disorder theory. The nonmodified irreversibility line for the low oxygenation regime samples allow us to confirm that the new defects created during the HOP process act as point pinning centers. On the other hand, the strong decrease in the irreversibility line after the high ΣO_2 regime evidences that in-plane dislocations and stacking faults are competing defects and that the effect of dislocations can be counterbalanced by wide stacking faults that enhance vortex cutting. We have also studied the field dependence of the critical current density for temperature $T \geqslant 45$ K. We remark that the differences in J_c introduced by the microstructural changes are principally localized in the low-field region (i.e., $H \leqslant 1.5$ T). A simple model based on single vortex pinning by dislocation cores has given good agreement with our experimental results, thus supporting the proposed separation methodology for the analysis of the critical currents in melt-textured $YBa_2Cu_3O_7$. As a final conclusion, we would like to stress that the present work has proposed a clear and straightforward methodology to sort out the different pinning contributions of 123/211 interfaces and in-plane dislocations in melt-textured $YBa_2Cu_3O_7$ which behave very differently as shown in this paper. The clarification of the pinning mechanisms of melt-textured YBCO materials will allow to further develop the processing techniques for optimizing the superconductive properties.

ACKNOWLEDGMENTS

Financial support from Supercurrents (Grant No. EU-TMR ERBFMRXCT98-0189), CICYT (Grant No. MAT99-0855), and Generalitat de Catalunya through the PIC-CIRIT program is acknowledged. We thank J.A. Alonso and M.J. Martinez for the use of a high oxygen pressure furnace facility.

*Electronic address: jerome@icmab.es;
URL: http://www.icmab.es/dmag/

[1] K. Salama, V. Selvamanickan, and D. Lee, *Processing and Properties of High T_c Superconductors*, edited by S. Sin (World Scientific, Singapore, 1993), Vol. 1.

[2] V. Selvamanickam, M. Mironova, and K. Salama, J. Mater. Res. **8**, 249 (1993).

[3] A. Leenders, M. Ullrich, L. Kautschor, and H. Freyhardt, J. Mater. Res. **14**, 354 (1999).

[4] P. McGinn, W. Chen, N. Zhu, L. Tan, C. Varanasi, and S. Sengupta, Appl. Phys. Lett. **59**, 120 (1991).

[5] E. Mendoza, T. Puig, E. Varesi, A.E. Carrillo, J. Plain, and X. Obradors, Physica C **334**, 7 (2000).

[6] M. Murakami, S. Gotoh, H. Fujimoto, K. Yamaguchi, N. Koshizuka, and S. Tanaka, Supercond. Sci. Technol. **4**, 43 (1991).

[7] B. Martinez, X. Obradors, A. Gou, V. Gomis, S. Pinol, J. Fontcuberta, and H. Van Tol, Phys. Rev. B **53**, 2797 (1996).

[8] V. Pan, in *Physics and Materials Science of Vortex States, Flux Pinning and Dynamics*, Vol. 26 of *NATO Advanced Studies Institute, Series B: Physics*, edited by R. Kossowsky, S. Bose, V. Pan, and Z. Durusoy (Plenum, New York, 1999), p. 1.

[9] Y. Feng, J.G. Wen, A.K. Pradhan, N. Koshizuka, and L. Zhou, J. Phys.: Condens. Matter **12**, 5843 (2000).

[10] Y. Zhang, M. Mironov, J. Lee, and K. Salama, Jpn. J. Appl. Phys., Part 1 **34**, 3077 (1995).

[11] T. Puig, J. Plain, F. Sandiumenge, X. Obradors, J. Rabier, and J. Alonso, Appl. Phys. Lett. **75**, 1952 (1999).

[12] B. Martinez, F. Sandiumenge, T. Puig, X. Obradors, L. Richard, and J. Rabier, Appl. Phys. Lett. **74**, 73 (1999).

[13] J. Plain, T. Puig, F. Sandiumenge, X. Obradors, J. Alonso, and J. Rabier, in *Applied Superconductivity*, Institute of Physics Conference Series, Vol. 167, edited by X. Obradors, F. Sandiumenge, and J. Fontcuberta (Institute of Physics, Bristol, 2000), p. 55.

[14] X. Obradors, R. Yu, F. Sandiumenge, B. Martinez, N. Vilalta, V. Gomis, T. Puig, and S. Pinol, Supercond. Sci. Technol. **10**, 884 (1997).

[15] E. Gyorgy, R. van Dover, K. Jackson, L. Schneemeyer, and J. Waszczak, Appl. Phys. Lett. **55**, 283 (1989).
[16] H. Wiesinger, F. Sauerzopf, and H. Weber, Physica C **203**, 121 (1992).
[17] R. Williams, K. Alexander, J. Brynestad, T. Henson, D. Kroeger, T. Lindemer, G. Marsh, and J. Scarbrough, J. Appl. Phys. **67**, 6934 (1990).
[18] R. Williams, K. Alexander, J. Brynestad, T. Henson, D. Kroeger, T. Lindemer, G. Marsh, J. Scarbrough, and A. Specht, J. Appl. Phys. **70**, 906 (1991).
[19] F. Sandiumenge, T. Puig, J. Rabier, J. Plain, and X. Obradors, Adv. Mater. **12**, 375 (2000).
[20] S.J. Rothman, J.L. Routbort, and J.E. Baker, Phys. Rev. B **40**, 8852 (1989).
[21] S.J. Rothman, J.L. Routbort, U. Welp, and J.E. Baker, Phys. Rev. B **44**, 2326 (1991).
[22] T. Tafto, M. Suenaga, and R. Sabatini, Appl. Phys. Lett. **52**, 667 (1988).
[23] J. Rabier, P. Tall, and M.F. Denanot, Philos. Mag. A **67**, 1021 (1993).
[24] J. Rignalda, C. Kiely, P. Fox, and G. Tatlock, Philos. Mag. A **69**, 729 (1994).
[25] H. Zanbergen, R. Gronsky, K. Wang, and G. Thomas, Nature (London) **331**, 596 (1988).
[26] F. Sandiumenge, N. Vilalta, S. Pinol, B. Martinez, and X. Obradors, Phys. Rev. B **51**, 6645 (1995).
[27] P. Hirsch, A. Howie, R. Nicholson, D. W. Pashley, and N. J. Whelan, *Electron Microscopy of Thin Crystals*, 2nd ed. (Krieger, Malabar, FL, 1977).
[28] D. Hull and D. J. Bacon, *Introduction to Dislocations*, 3rd ed. (Butterworth-Heinemann, Oxford, 1984).
[29] H. Ledbetter and M. Lei, J. Mater. Res. **6**, 2253 (1991).
[30] A. Goyal, W. Oliver, P. Funkenbusch, D. Kroeger, and S. Burns, Physica C **183**, 221 (1991).
[31] M. Fendorf, C. Burmester, L. Wille, and R. Gronsky, Appl. Phys. Lett. **57**, 2481 (1990).
[32] D.S. Fisher, M.P.A. Fisher, and D.A. Huse, Phys. Rev. B **43**, 130 (1991).
[33] G. Blatter, M. Feigel'man, V. Geshkenbein, A. Larkin, and V. Vinokur, Rev. Mod. Phys. **66**, 1125 (1994).
[34] D.R. Nelson and V.M. Vinokur, Phys. Rev. B **48**, 13 060 (1993).
[35] S. Sanfilippo, D. Bourgault, C. Villard, R. Tournier, P. G. Picard, E. Beaugnon, A. Sulpice, T. Fournier, and P. Germi, Europhys. Lett. **39**, 657 (1997).
[36] S. Sanfilippo, A. Sulpice, O. Laborde, D. Bourgault, T. Fournier, and R. Tournier, Phys. Rev. B **58**, 15 189 (1998).
[37] B. Martinez, T. Puig, A. Gou, S. Pinol, J. Fontcuberta, X. Obradors, and H. Van Tol, Phys. Rev. B **58**, 15 198 (1998).
[38] T. Puig, F. Galante, E.M. Gonzalez, J.L. Vicent, B. Martinez, and X. Obradors, Phys. Rev. B **60**, 13 099 (1999).
[39] H. Suematsu, H. Okamura, S. Nagaya, and H. Yamauchi, Supercond. Sci. Technol. **12**, 274 (1999).
[40] L. Civale, A. Marvic, M. MacElfresh, T. Worthington, A. Malezemof, F. Holtzberg, J. Thompson, and M. Kirk, Phys. Rev. Lett. **65**, 1164 (1990).
[41] X.G. Qiu, V.V. Moshchalkov, Y. Bruynseraede, and J. Karpinski, Phys. Rev. B **58**, 8826 (1998).
[42] X.G. Qiu, V.V. Moshchalkov, and J. Karpinski, Phys. Rev. B **62**, 4119 (2000).
[43] M. Ullrich, D. Muller, W. Mexner, M. Steins, K. Heinemann, and H.C. Freyhardt, Phys. Rev. B **48**, 7513 (1993).